Acoustic Properties of Aircraft Wake Vortices

P. Böhning[1], U. Michel[2] and R. Baumann[3]
[1] Rolls-Royce Deutschland Ltd & Co KG, Dahlewitz, Eschenweg 11,
D-15827 Blankenfelde-Mahlow, Germany
[2] Deutsches Zentrum für Luft- und Raumfahrt (DLR), Institute of Propulsion Technology,
Müller-Breslau-Str. 8, D-10623 Berlin, Germany
[3] Deutsches Zentrum für Luft- und Raumfahrt (DLR), Institut für Physik der Atmosphäre,
Oberpfaffenhofen, D-82234 Wessling, Germany

ABSTRACT

The noise generation by aircraft wake vortices has been studied numerically and experimentally. The numerical study revealed a relation between the circulation Γ, the vortex core size r_c and the frequency f_a of the peak level in the vortex noise spectra, $f_a \approx \Gamma/(2\pi r_c)^2$. The experimental data were obtained in measurements at airports applying phased microphone arrays. It has been revealed that sound sources are closely located to the vortex cores. The focused noise spectra of the wake vortices of all measured aircraft types are dominated by two maxima. The second maximum at f = 100 Hz is clearly caused by wake vortices. The origin of the first at 12 Hz has not been identified. Wake vortices were acoustically detected in 80 percent of the flyovers. Lowest detection rates were observed for the newer aircraft types Airbus 319, 320 and Boeing 737-800. A comparison of the wake trajectories obtained by phased microphone arrays and LIDAR revealed that the detection capability of the latter is superior.

1. INTRODUCTION

Aircraft wake vortices represent a major constraint for the separation of consecutive aircraft en-route and in terminal areas. The current aircraft separation rules for landing and take-off defined by the *International Civil Aviation Organisation (ICAO)* in 1971 [1], already represent an important capacity limiting factor at congested airports. The rules categorize aircraft into four maximum take-off weight classes, *light*, *medium*, *heavy* and a recently introduced class for the Airbus A380. The minimal separation distance depends only on the combination of the weight classes of the leading and following aircraft ignoring the actual wake vortex behaviour which varies between different aircraft types and depends strongly on the actual meteorological conditions as demonstrated in several studies conducted in the recent years [2].

The expected increase in air traffic makes a reduction of the aircraft separation without negative effects on the safety level highly desirable. This in turn demands precise knowledge of the wake vortex structure and its evolution under different meteorological conditions. To gain this knowledge an intense research effort has been undertaken in the *European Union (EU)* and in the *United States (US)* to develop reliable wake vortex prediction methods and detection technologies in recent years. A number of flyover measurement campaigns were conducted in which LIDAR has become the standard technique for measuring the wake vortex parameters in field tests. A complimentary detection technology has attracted researchers' interest after the observation that wake vortices emit a faint noise which varies with the aircraft type generating the vortices. The wake vortex noise is therefore expected to provide additional information about wake vortex characteristics in flyover test.

The *German Aerospace Center (DLR)* proposed the application of a phased microphone array for the investigation of wake vortex noise. In contrast to a single microphone a phased microphone array allows to distinguish between noise originating from the wake vortex, the aircraft and from other sources on the ground. The capability of phased microphone arrays to localize the noise sources of wake vortices was first demonstrated in a test at Berlin's *Airport Schönefeld* in 2000 [3]. In a second test, conducted in Tarbes, France, in 2002, phased microphone arrays were applied to study the wake vortex noise of an Airbus 340 which was flown in different configurations and with different engine settings [4]. Both tests were conducted in the framework of the European research project *C-Wake*.

At the same time, similar activities took place in the *US* as part of a research project. Its objective was the development and evaluation of alternative wake detection technologies such as *phased microphone arrays*, *opto-acoustic microphones*, *Continuous LIDAR* and *Pulsed LIDAR*. These technologies were evaluated in a field test at the *Denver International Airport* organized by the *NASA Langley Research Center* and the *Volpe Center, Department of Transportation (DoT)* in 2003, [5]-[8]. *DLR* participated applying a phased microphone array.

Currently, studies on wake vortex noise concentrate on identifying the dominant noise generating mechanisms in the vortices and on finding a governing relation between aerodynamic wake parameters such as circulation and core size and the spectral and temporal characteristics of the vortex noise using experimental and numerical data.

2. WAKE VORTEX LIFE CYCLE AND SOUND GENERATING MECHANISMS

The life cycle of an aircraft wake vortex consists of a roll-up, diffusion and a rapid decay phase [9]. The roll-up phase comprises the shedding of concentrated and distributed vorticity by the aircraft, an intense vorticity interaction and the final roll up to two strong counter-rotating vortices. This process is finished within $x < 10$ B, where B refers to the aircraft's wing span. The acceleration of vorticity is expected to be the main source of sound in this early state of vortex life.

During the diffusion phase the counter-rotating vortices remain stable and move slowly downwards due to the mutually induced velocity. The generation of noise by wake vortices in this phase surprises as it is well-known that slowly moving potential vortices do not emit any sound. However, there are two potential noise generating mechanisms. First, a spinning Kirchhoff-vortex, having an elliptical core of uniform vorticity does emit a tone at a frequency equal to the double of the vortex rotation frequency. So, it can be expected that any perturbation of a homogeneous vorticity distribution in one of the two rotating vortex cores is a potential source of sound. The noise produced should be in the same frequency range as the rotation frequency of the vortex cores [10]. Second, the likely more important mechanism is the interaction of secondary vorticity structures (SVS) with the two main vortices which are referred to as primary vorticity structures (PVS). This interaction is also believed to be the main decaying mechanism in aircraft wake vortices [11]. SVS are turbulent eddies from the atmospheric turbulence or engine exhaust jets which interact with the swirling mean flow field of the PVS. These eddies are getting stretched and tilted in the mean flow [11],[12] and accelerated as they are getting closer to the cores of the main vortices. Accelerated vorticity is an effective sound source.

The rapid decay phase is predominated by instability effects that cause the wake vortex to rapidly break up. Responsible instability effects must provoke sufficiently large

amplitudes of perturbation. Mechanisms providing only small perturbation amplitudes may provoke local vortex busting. These instabilities are often recognised as sharp whipping noise. Instability mechanisms which provoke displacements of the vortex cores in the range of the vortex spacing cause linking of the two primary vortices and a formation of vortex rings.

3. NUMERICAL STUDY

The generation of sound by the interaction of SVS with PVS was studied on a four-vortex system as shown in **FIG 1**. This configuration may be used as a simplified model for the vortices shed from wing tips and outer flap edges, which quickly merge into a strong outer vortex pair, and the counter-rotating vortices shed from the inner flap edges forming a second, weaker vortex pair. The behaviour of such a system, i.e. weak or strong interaction of the vortex filaments, is described by the Donaldson-Bilanin diagram [13]. It depends on the ratio of the initial circulation of the outer (1) and inner (2) vortex filaments Γ_2/Γ_1 and the ratio of their initial spacing b_2/b_1. The ratio of the initial circulation was set to Γ_2/Γ_1 = -0.3 (Γ_1=1) and of the initial vortex spacing b_2/b_1 = 0.3. The negative sign of the circulation ratio indicates that the outer and inner vortex filaments are counter-rotating. The weaker vortex filaments are expected to strongly interact with the corresponding main vortices. An initial disturbance consisting of a sinusoidal displacement of the vortex cores with an amplitude of a_0=0.0001 b_1 and wave length λ = 0.98 b_1 along their axis was applied to trigger the development of instabilities. The 3D-LES was performed by *DLR Institute of Atmospheric Physics* using its in-house incompressible *LESTUF* code [14]. The original LES was performed in the framework of the European research project *AWIATOR*.

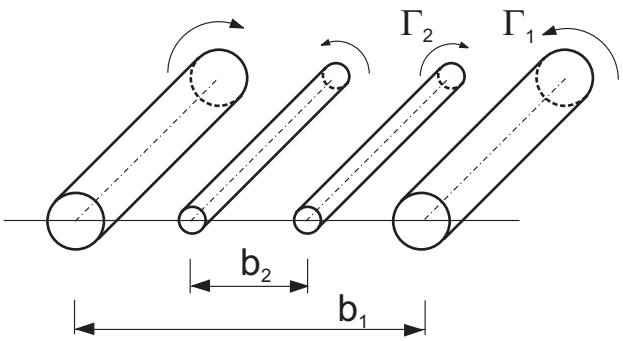

FIG 1: Four-vortex system used for study of wake vortex noise

The LES was carried out in two steps. First, the simulation was run for a long time interval but with a low time resolution to identify the main flow features. Second, a smaller interval interesting for the noise study was re-calculated with a higher time resolution. The second calculation was initialised with the flow field obtained in the first simulation. A domain size of $L_x \times L_y \times L_z$ = 4.8 $b_1 \times$ 0.98 $b_1 \times$ 8 b_1 with a grid spacing of $\Delta y/b_1$ = 0.01536 in the direction of flight and $\Delta x/b_1 = \Delta z/b_1$ = 0.0125 in the spanwise x and the vertical direction z was chosen. The vortex core radii are r_{c1} = 0.075 b_1 and r_{c2} = 0.05 b_1. The time resolution of the first simulation was $\Delta t^* = \Delta t/t_0 = 3.18*10^{-4}$, with $t_0 = 2\pi\, b_1^2/\Gamma_1$.

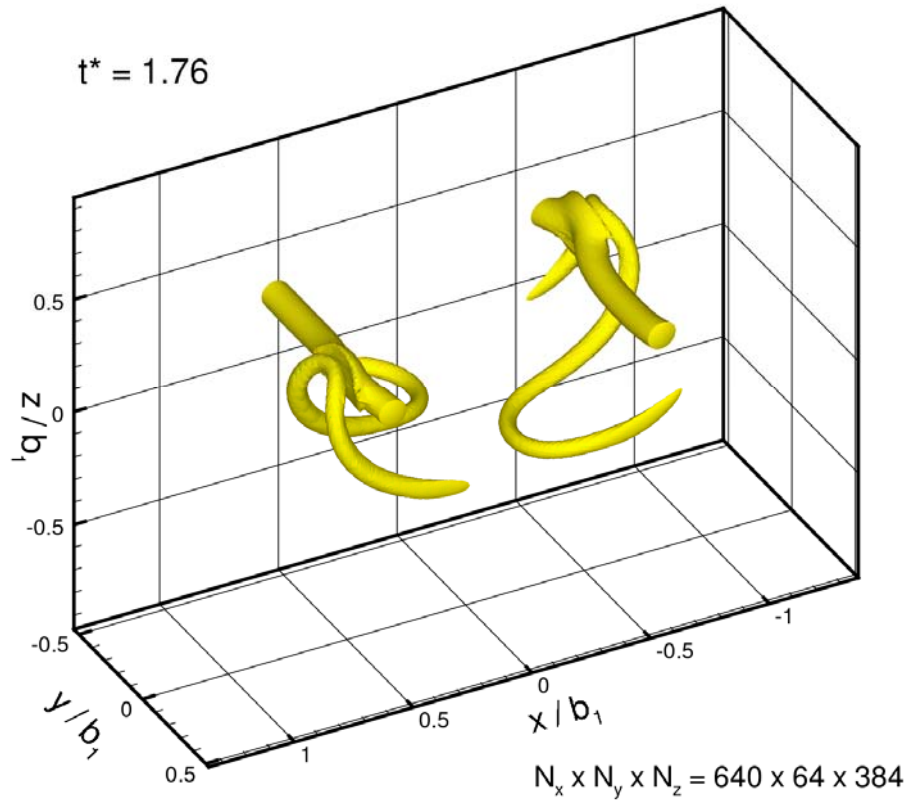

FIG 2: Normalized λ_2*-surfaces of the simulated four-vortex system at normalized time t* = 1.76

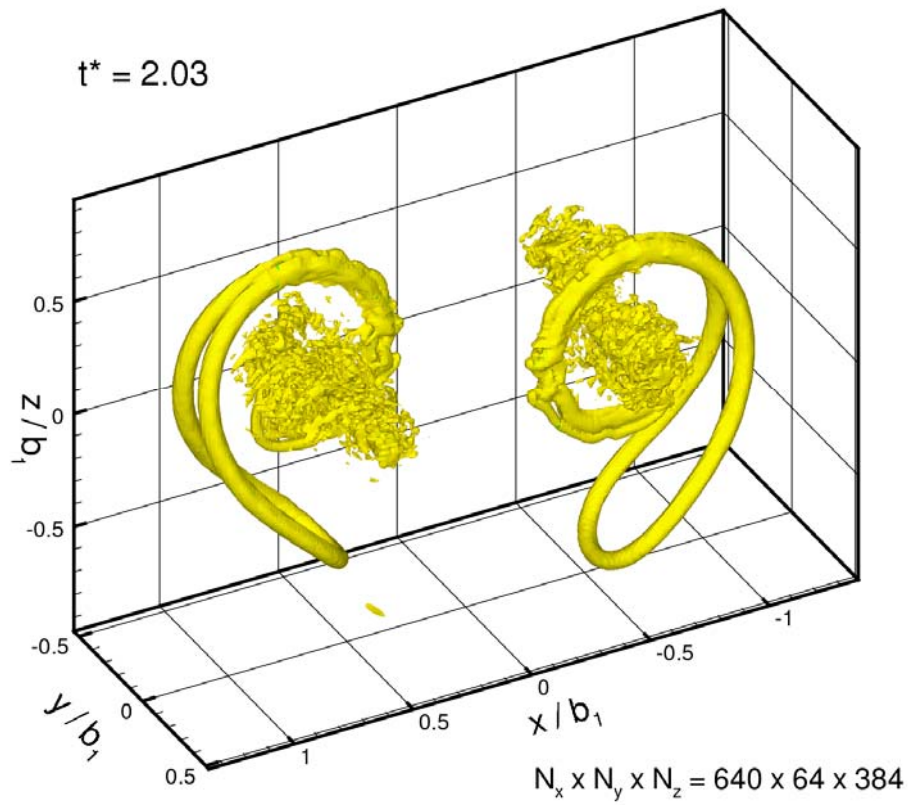

FIG 3: Normalized λ_2*-surfaces of the simulated four-vortex system at normalized time t* = 2.03

FIG 2 and **FIG 3** show the normalized λ_2*-surfaces [15] of the four-vortex system at two instants of normalized time, t* = 1.76 and t* = 2.03. At the beginning of the simulation the weaker vortex starts to slowly rotate around its corresponding primary vortex. Due to the initial displacement of the vortex cores the weaker filaments experience varying acceleration along their axes and become consequently deformed. As long as the spacing between stronger and weaker vortices is large, the weaker rotate slowly around the stronger filaments. At t* = 1.76, however, a short segment of the weaker filament touches the core of the stronger vortex and starts to rotate at a much higher speed $v_\theta = v_\theta(r \approx r_{c1})$ around the mean vortex. The resulting in-homogenous vorticity distribution close to the core of the main vortex is expected to produce sound at frequencies close to the rotation frequency of the core f_r.

A few rotations later finer scale turbulence produced by the strong interaction is found to be distributed around the surviving outer filaments. This fine-scale turbulence is believed to produce sound at frequencies above the rotation frequency of the main vortex cores.

The flow field was de-normalised with the parameters of a landing Bombardier CRJ200 aircraft at t* = 1.69. The parameters are aircraft weight m = 19100 kg, wing span B = 21.2 m and landing speed v = 80m/s. Assuming an elliptical lift distribution the vortex spacing is $b_1 = \pi/4 = 16.7$ m and the initial vortex sink rate $w_0 = b_1 / t_0 = 1.28$ m/s. The resulting distributions of the vorticity ω_y and the velocity v_z along a line across the vortex cores at t* = 1.69 are plotted in **FIG 4**. v_z is asymmetric since the profile is offset by the sink speed of the vortex system. The core radius is estimated from the distance between the turning points in the velocity profile to be of $r_c \approx 0.1\ b_1$. The maximal tangential velocity is $v_\theta\ (r = r_{c1}) \approx 12$ m/s. A rotation frequency of $f_r = 1.1$ Hz results.

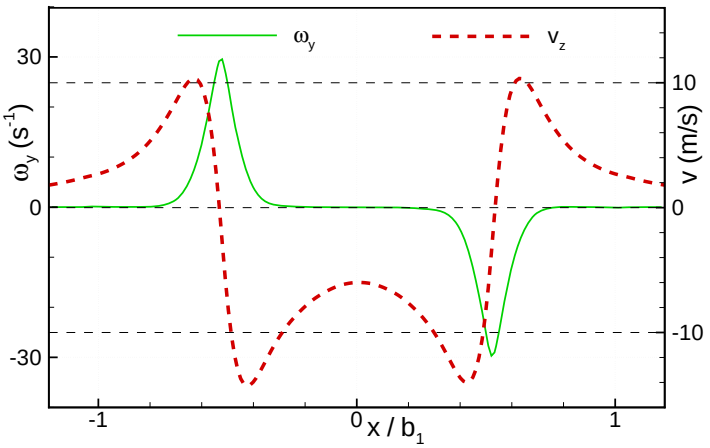

FIG 4: Vorticity ω_y and velocity v_z distribution along a line crossing the vortex cores

The generation of vortex sound in flows with small Mach numbers M « 1 and large Reynolds numbers Re » 1 is described by equation (1). This far-field solution of *Lighthill's* equation was first derived by *Powell* [17] and later studied in more detail by *Howe* [18]. x refers to the observer position, *v* to the local flow velocity and ρ_0 to the mean flow density. The term in brackets is evaluated at retarded time $t_r \approx t - |\vec{x} - \vec{y}| / c_0$.

Equation (1) states that only accelerated vorticity ω generates sound. Vorticity at rest is silent. The term in the integral together with the LES solution suggests that the dominant sound sources are located where the SVS touches the PVS and experience their highest accelerations.

$$p(\vec{x},t) = \frac{-\rho_0 x_i}{4\pi c_0 |\vec{x}|^2} \frac{\partial}{\partial t} \int \left[(\vec{\omega} \times \vec{v}) \right]_i d^3\vec{y} \qquad (1)$$

A significant advantage of this formulation over the far-field solution based on the *Lighthill*-Tensor is that the volume integral is limited to a relative small region where strong vorticity ω is found. A second far-field solution, equation (2), was derived by *Möhring* [19] by the assumption that the sound source is acoustically compact. This formulation has been applied for the calculation of the far-field wake vortex noise in the present study.

$$p(\vec{x},t) = \frac{-\rho_0 x_i x_j}{12\pi c_0^2 |\vec{x}|^3} \frac{\partial^3}{\partial t^3} \int y_i \left(\vec{y} \times \vec{\omega} \right)_j (\vec{y}, t - |\vec{x}| / c_0) d^3\vec{y} \qquad (2)$$

The integral is evaluated at an approximated retarded time $t_r \approx t - |\vec{x}|/c_0$. *Möhring's* far-field solution is valid for small Mach numbers M « 1 and large Reynolds numbers Re » 1. A significant disadvantage of this formulation is the numerical noise produced by the third derivative with respect to the time *t*. The LES dedicated to the noise study was run with a higher time resolution of $\Delta t^* = 3.18 \cdot 10^{-5}$ in the interval $t^* = 1.69 \ldots 2.07$. Only a reduced domain containing significant vorticity of size $L_x \times L_y \times L_z = 2.5\ b_1 \times 0.98\ b_1 \times 1.75\ b_1$ has been evaluated.

FIG 5 shows the calculated power spectral density. It is dominated by a hump at f ≈ 0.9 Hz which is very close to the estimated rotation frequency of the core f ≈ 1.1 Hz. In experiments the peak levels are found at much higher frequencies, $f_1 \approx 10$ Hz and $f_2 \approx 100$ Hz. The origin of the peak in experimental data at f_2 is certainly the wake vortex although the source of the first peak is still in question. The discrepancy between the peak frequencies found in the numerical study and the experimental results is probably caused by the core radii used in the simulation. Unfortunately, the minimal feasible core radii in the simulation were limited by computational restrictions. Smaller core radii would require a higher spatial resolution which in turn means a longer calculation time. Smaller core radii, however, would let the SVS rotate around the outer filaments at higher speed. As a consequence, the hump in the spectra would appear at higher frequencies.

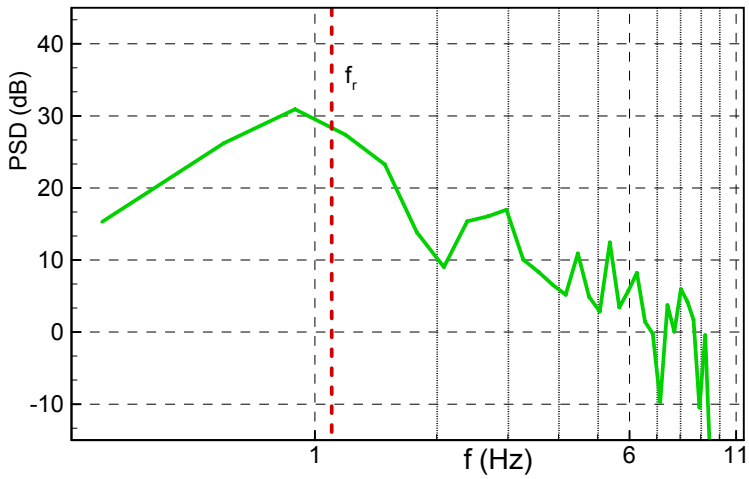

FIG 5: Wake vortex noise spectrum average over an interval of length Δt=3.2sec

The measurement of vortex core radii in fly-over test is still difficult and depends on the vortex model used for the data fit. Recent measurements, however, indicate much smaller core radii of $r_c \approx 0.01 \ldots 0.02$ B [16] than used in the LES. As the rotation frequency of a vortex is proportional to $1/r^2$, a core radius of $r_c = 0.013\ b_1$, corresponding to $r_c \approx 0.01$B assuming an elliptical lift distribution, would move the hump to f ≈ 53 Hz. This frequency is in the frequency range where peak levels were found in the experiments.

The numerically predicted level at the peak frequency is L = 28 dB. A normalization on the vortex length would give a correction of $\Delta L = -10\ log(L_y\ b_1\ /\ 1m) = -12\ dB$. The numerically predicted level L = 16 dB and L = 10 ... 20 dB observed in measurements are in surprisingly good agreement, especially when recalling that the circulation ratio of $\Gamma_2/\Gamma_1 = -0.3$ used in the LES is much higher than expected in real wake vortices.

4. EXPERIMENTAL SET-UP AND DATA REDUCTION

The *DLR (German Aerospace Center)* participated in several flyover measurements applying phased microphone arrays for the localization and the characterization of aircraft wake vortices. The experimental results obtained with two complimentary arrays, in the following called T- and X-array, are discussed in the next section. The first consisted of 128 low-cost microphones pre-installed on 4 boards each of size 1.2 x 1.7 m. The second consisted of 64 microphones equally spaced on the two arms of a cross each of D = 40 m length.

The microphone signals of the T-array were processed by the *classical beamforming* algorithm in the time domain providing the noise source distributions of the wake vortex in 1/3-octave bands. An X-array offers some practical advantages concerning the installation and good sidelobe suppression between the two axes. Unfortunately, high sidelobes emerge along the axes which, however, can be suppressed by a modified algorithm. This modified method was developed for the processing in the frequency domain [19] and later adopted to the time domain [21]. The underlying idea is to remove these elements from the cross-spectral matrix which were calculated from the signal of microphones belonging to the same arm of the cross-array. In the time domain this reads, first, the *classical beamforming* is performed for the microphones of each arm separately. Second, the two focused time signals $b_A(y,t)$ and $b_B(y,t)$ are cross-correlated, equation (3a), which results in a single value $s(y, \tau = 0)$ describing the broadband sound energy content originating from the focus point. A spectral estimation requires (i) filtering of the two focused time signals $b_A(y,t)$ and $b_B(y,t)$ or (ii) calculating the Fourier transformed $B_A(y,\omega)$ and $B_B(y,\omega)$ before cross-correlating. The latter provides a narrow band spectrum of the sound energy radiated from the focus point.

$$s(\vec{y}, \tau = 0) = \sum_{n=1}^{N} b_A(\vec{y}, t_n) b_B(\vec{y}, t_n) \tag{3a}$$

$$or: \qquad S(\vec{y}) = B_A^*(\vec{y}, \omega)\, B_B(\vec{y}, \omega) \tag{3b}$$

The cross-correlation matrix may not remain *positive-definite* after the modification which could result in negative radiated energy for certain focus positions. It can be assumed that if negative energy occurs at a focus point then no dominant source is located at this position. Hence, a simple maximum condition was introduced setting negative values to zero.

(4a)

$$s^{\mathrm{mod}}(\vec{y}) = \max\{s(\vec{y}),0\}$$

$$or: \quad S^{\mathrm{mod}}(\vec{y}) = \max\{S(\vec{y});0\} \tag{4b}$$

This means that no information was obtained for these focus points. Taking the absolute values as energy content would lead to wrong results.

5. DISCUSSION OF THE EXPERIMENTAL RESULTS

The experimental results presented below are based on the microphone array data measured by *DLR* in a field test at the *Denver International Airport* organized by the *NASA* and the *DoT* in 2003 [5]-[8]. LIDAR and weather data were provided by *NASA, DoT* and *Flight Safety Technologies Inc. (FSTI)*. In the discussion below the ICAO aircraft types codes are used which are summarized in TAB 2 of the appendix.

5.1. Source distribution in horizontal plane

FIG 6 and **FIG 7** show the evolution of the sound source distribution in the wake vortex behind an aircraft of type B733 in the 1/3-octave bands f = 160 Hz and f = 80 Hz respectively. The four time intervals evaluated are centred at t = 4.7, 7.9, 11.1 and 14.2 sec after the aircraft flyover. Each interval has a length Δt = 1.57 sec. The aircraft crossed the microphone array in x-direction at an altitude of h = 200 m and a speed of v = 80 m/s. The scan altitude was adjusted to the current wake vortex altitude which was derived from LIDAR measurements.

The source distributions in **FIG 6** reveal a concentration of noise sources with varying intensity along two parallel lines in flight direction. These lines are associated with the position of the cores of the two main vortices. It was concluded that the noise sources are located close to or at the main vortex cores. This in turn allows the two vortices of an aircraft wake vortex to be localised and tracked separately. It also meets the expectations from the numerical study where the vorticity in the vicinity of the core was identified as potential sound source.

The variation of source intensity along the lines was also observed in other measurements where different microphone arrays and processing techniques were applied. Therefore, the variation of the source intensity is believed to be an inherent property of wake vortices. At lower frequencies (**FIG 7**) the source intensity variations are less emphasised since a larger beam width of the microphone array causes the source distribution to be spatially averaged.

By changing the averaging time of the calculation varying source distributions were found which means that the source distribution is highly unsteady. It was concluded that the coherence time length is smaller than 1 sec for all frequency bands.

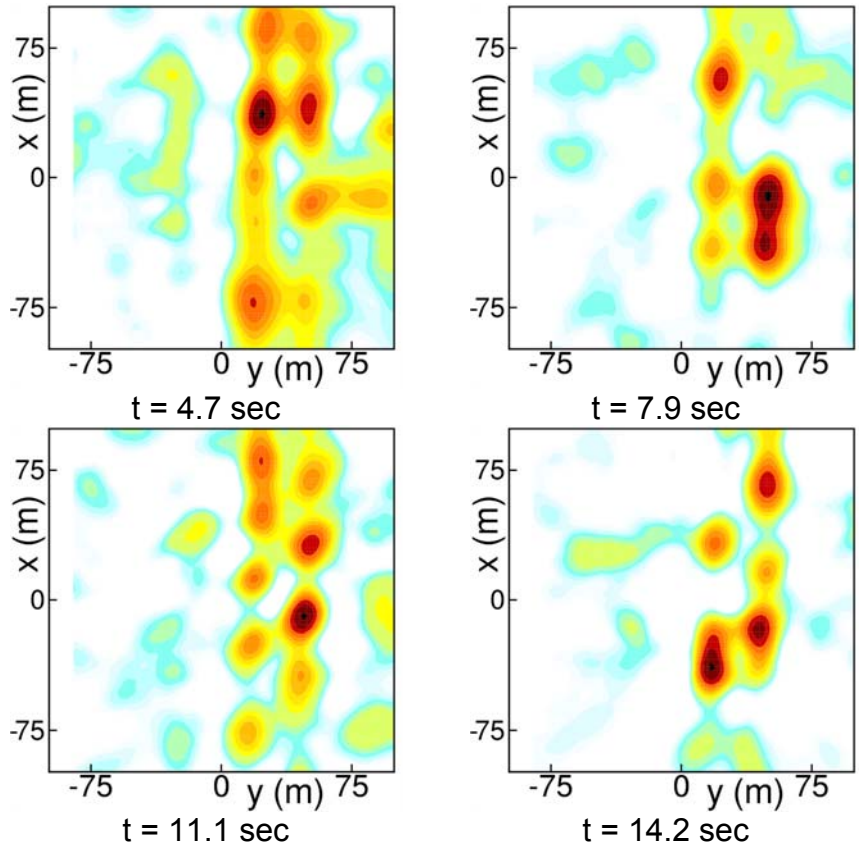

FIG 6: Source distribution in a 1/3-octave band f = 160 Hz in the wake vortex of an aircraft of type B733 at different times after fly-over

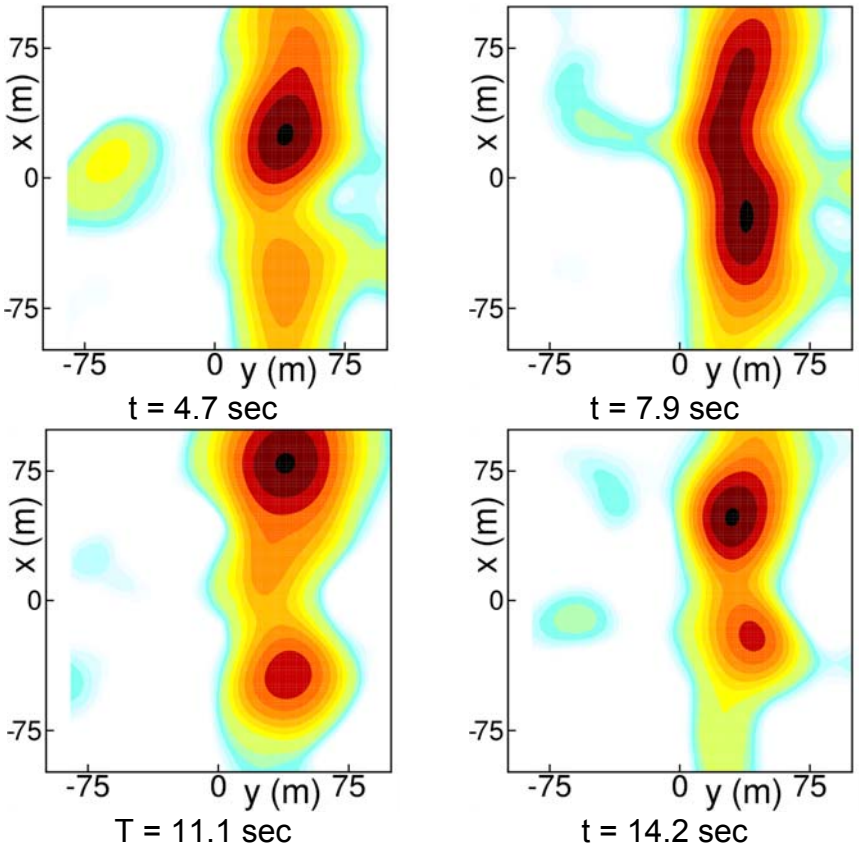

FIG 7: Source distribution in the 1/3-octave band f = 80 Hz the in the wake vortex of an aircraft of type B733 at different times after fly-over

5.2. Source distribution in vertical plane

As it was found that the sound sources are located close to the vortex cores a scan for sources in a vertical plane, the y-z plane, might allow the vortex altitude to be determined. Unfortunately the spatial resolution of a two-dimensional array in a direction perpendicular to the ground is very pour. An example of a scanned source distribution in the y-z plane for the wake vortex behind an aircraft of type B733 is given in

FIG 8. The flyover altitude was h = 180 m, marked in the plots by a dashed line, and the aircraft speed was v = 80 m/s. The vortex positions derived from simultaneously conducted LIDAR measurements are indicated in the plots by blue circles. The distributions are based on the data obtained by the X-array.

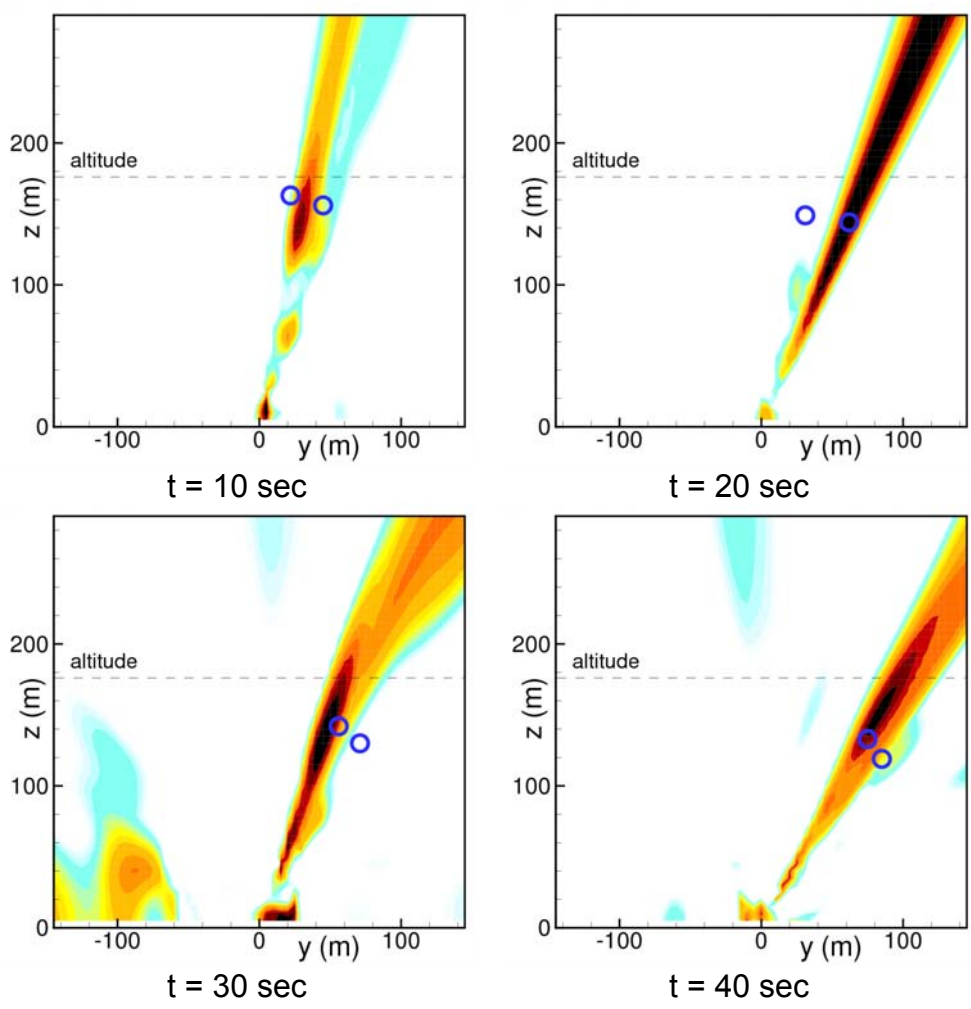

FIG 8: Source distribution in the y-z plane in the 1/3-octave band f = 200 Hz of a wake vortex behind an aircraft of type B733 at different times after fly-over

In some of the plots the maximal sound pressure level appears below and in others above the actual vortex position. The direction switches between left and right vortex. This switching can be avoided by an adopted averaging in space and time allowing both vortices to be tracked at the same time. It is believed that even a de-convolution algorithm would fail to detect the right vortex height. Larger microphone arrays provide better spatial resolution in vertical direction but also suffer from coherence loss between

largely spaced microphones. A more appropriate solution is seen in the application of two microphone arrays spaced a lateral distance similar to the aircraft height $\Delta y \approx z_{ac}$. The first microphone array would detect the wake vortices under an angle of $\varphi = 90°$ and the second of $\varphi = 45°$. Hence, the source altitude can be derived via triangulation.

It was mentioned above that the source distribution strongly depends on the averaging time used for the *beamforming*. Therefore, it is important that the source strength at each point of the plot is evaluated at its retarded time $t_r \approx t - |\vec{x} - \vec{y}| / c_0$. This is even more important when the source altitude is determined by means of the source positions in the x-y plane via triangulation.

5.3. Source distribution in the y-t plane

An important factor in terms of safety is the crosswind which transports the wake vortices out of the flight corridors. To observe the lateral transport of the wakes the source distribution scanned along a line perpendicular to the flight path and plotted as a function of time is very useful.

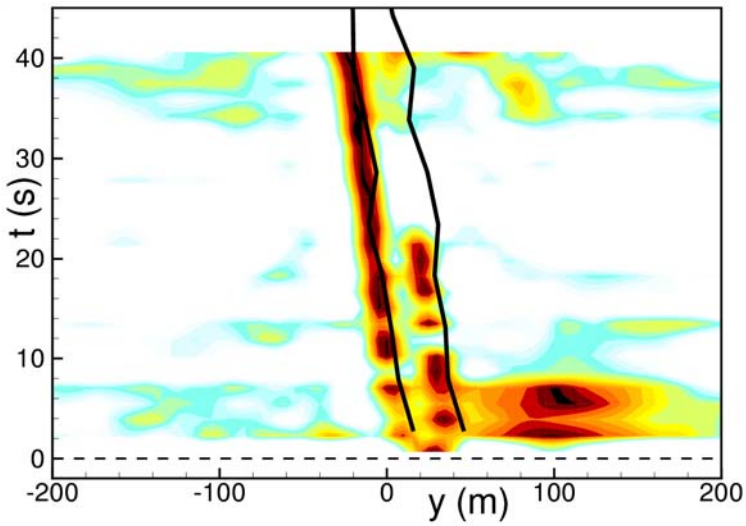

FIG 9: Source distribution in the y-t plane after a fly-over of an aircraft of type B733

In **FIG 9**, the lateral source distribution behind an aircraft of type B733 is plotted as a function of time. The aircraft crosses the microphone array centre at t = 0 sec which is indicated by a dotted line.

The vortex cores are recognized as non-continuous source distribution along two vertical lines. The source distribution is occasionally dominated by only one of the two vortices. If both vortices need to be tracked at the same, the dominance of only one vortex can be avoided by an adopted averaging in space and time. The black lines represent the vortex trajectories obtained by the LIDAR measurements. A slight offset between the LIDAR trajectories and the acoustic source distribution can be observed and was probably caused by an undocumented offset between the measurement systems.

5.4. Detection rate of the wake vortices

To evaluate the reliability of the sound emission of the wake vortices and its weather dependence the detection rates were determined. The source distributions in the y-t plane in all 1/3-octave bands between 40 Hz and 630 Hz of all flyovers were checked for clearly detectable wake vortices. For a graphical presentation in **FIG 10** the number of detected wakes is plotted as function of the flyover index number.

The detected wakes were counted at t = 10, 20, 30 and 40 sec after the flyover. The aircraft types were not distinguished. The test days are separated by vertical dashed lines. The graph shows that wake vortices were detected at t = 10 sec in about 85% of all flyovers. Only slightly less wake vortices were detected at t = 20 sec. The lines at t = 30 sec and t = 40 sec show a smaller gradient for the days D2 to D6 than for days D8 to D10. A correlation with the weather data revealed much higher wind speeds for the first period than for the second period.

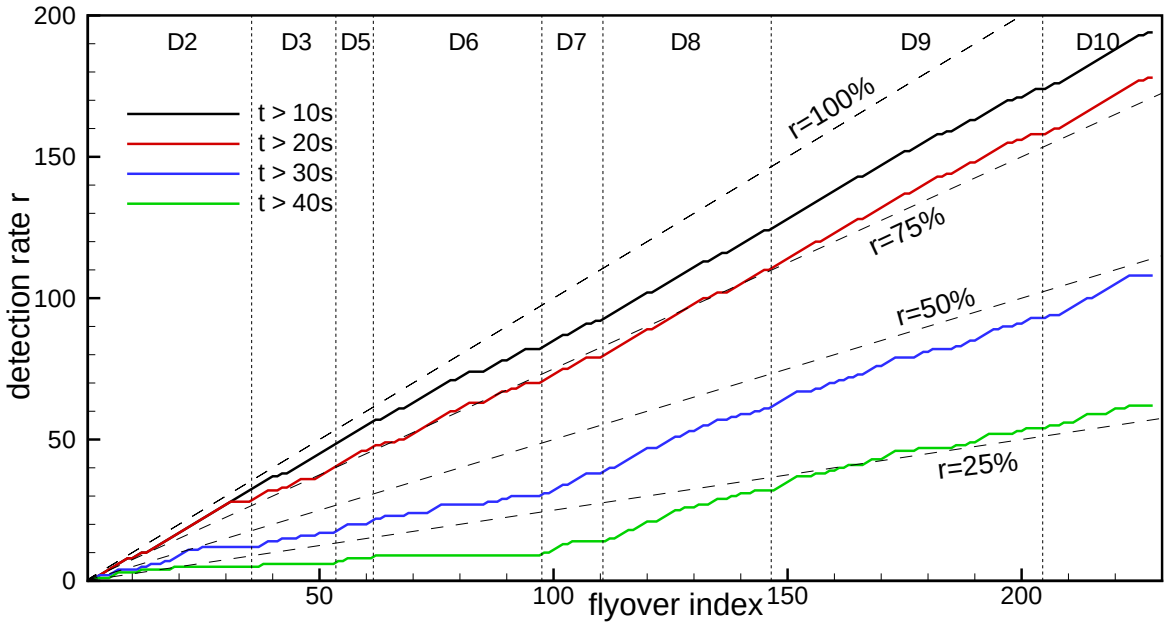

FIG 10: Number of detected wake vortices over the identification number of the measured flyovers

A correlation with the vortex trajectories obtained by LIDAR revealed that LIDAR detected vortices in nearly all flyovers. For some flyovers LIDAR was able to capture the vortices up to 20 sec longer that the phased microphone array. Despite the fact that LIDAR shows better detection capabilities, acoustic technologies are interesting as they are complimentary and still burry a huge potential for capability improvements.

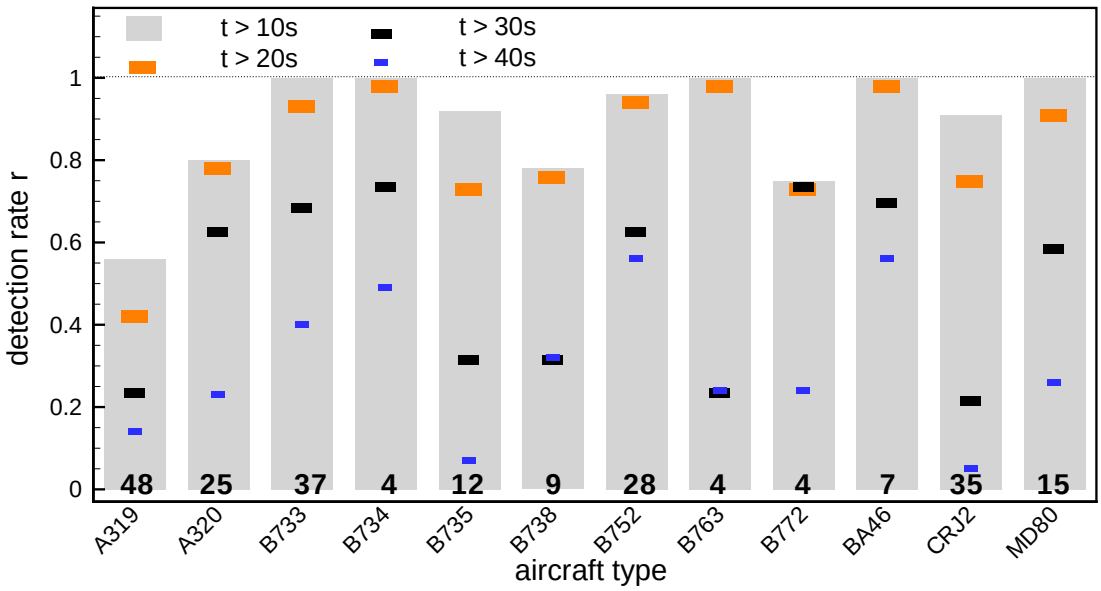

FIG 11: Wake vortex detection over aircraft type

FIG 11 shows the detection rate at four times after the aircraft flyover t = 10, 20, 30 and 40 sec for the different aircraft types. The detection rate is defined as the number of detected wakes divided by the total number of flyover of this type. The total number of flyovers of each type is plotted at the bottom of the graph.

It is interesting that the wake detection rate behind newer aircraft types such as A319, A320, B738 and B772 is obviously smaller than behind older types such as B733, B734, B763 and an MD80.

5.5. Normalized noise spectra

The narrow band spectrum of the wake vortex noise is expected to provide some characteristic spectral features such as the frequency at the peak level which are driven by flow parameters such as circulation and vortex core size.

The wake vortex noise spectra were obtained in two steps. First, the wake vortex tracks were derived from the *y-t* source distribution by means of a *Kalman* filter. Second, a spatial interval y = y0 $\pm$ Δy were defined for which i) the average power spectral density level PSD_a and ii) the highest peak level PSD_p was determined. A focused spectrum obtained by a *beamforming* method depends on the beam width of the microphone array. By normalizing the spectrum on the frequency *f* or wavelength λ, the array dimension *D*, source distance *r* and a characteristic array factor x_g this dependence can be eliminated. As the source distribution only extents in flight direction the spectra were normalised only on the array extension in flight direction.

$$\Delta L = -10\log(x_g \lambda r / D) \tag{5}$$

The wake vortex noise spectra of 13 flyovers of the aircraft type B733 were compared at different times after flyover and found to be very similar in level and in its characteristics. **FIG 12** shows the normalised focused PSD_a (XA and TA) and PSD_p (XAM) spectra of the wake vortex noise for the aircraft type B733 at t = 10 sec and t = 25 sec. The spectra were obtained by averaging the PSD_a and PSD_p spectra of 13 flyovers. The

standard deviations added to the mean values are plotted as dashed lines. The frequency range f < 220 Hz is covered by the X-array (XA) and f > 220 Hz by the T-array (TA). The prefect match between the PSD_a-spectra of the XA and TA at f = 220 Hz proves the suitability of the normalisation. The PSD_p spectra were plotted as they stronger pronounce the level maxima. The PSD_p spectra of the XA and TA do not match at the f = 220 Hz as the peak levels depend on the array beam width even if the normalisation is applied.

The measured wake vortex noise spectra have two characteristic maxima: a weaker one around $f_1 \approx 12$ Hz and a stronger one around $f_2 \approx 100$ Hz. The source of the second has been clearly identified in the source distribution of the corresponding 1/3 octave band of all 13 flyovers to be the wake vortices. The hump moves towards lower frequencies as the wake ages. The origin of the first maximum has not been identified. Unfortunately, the XA is too small to allow localising the sound source in this frequency range. A much larger microphone array would be required for a reliable source localisation. The levels at all frequencies decrease with time. The narrow peaks at f = 30, 60, 120, 180 Hz are caused by the electric power supply.

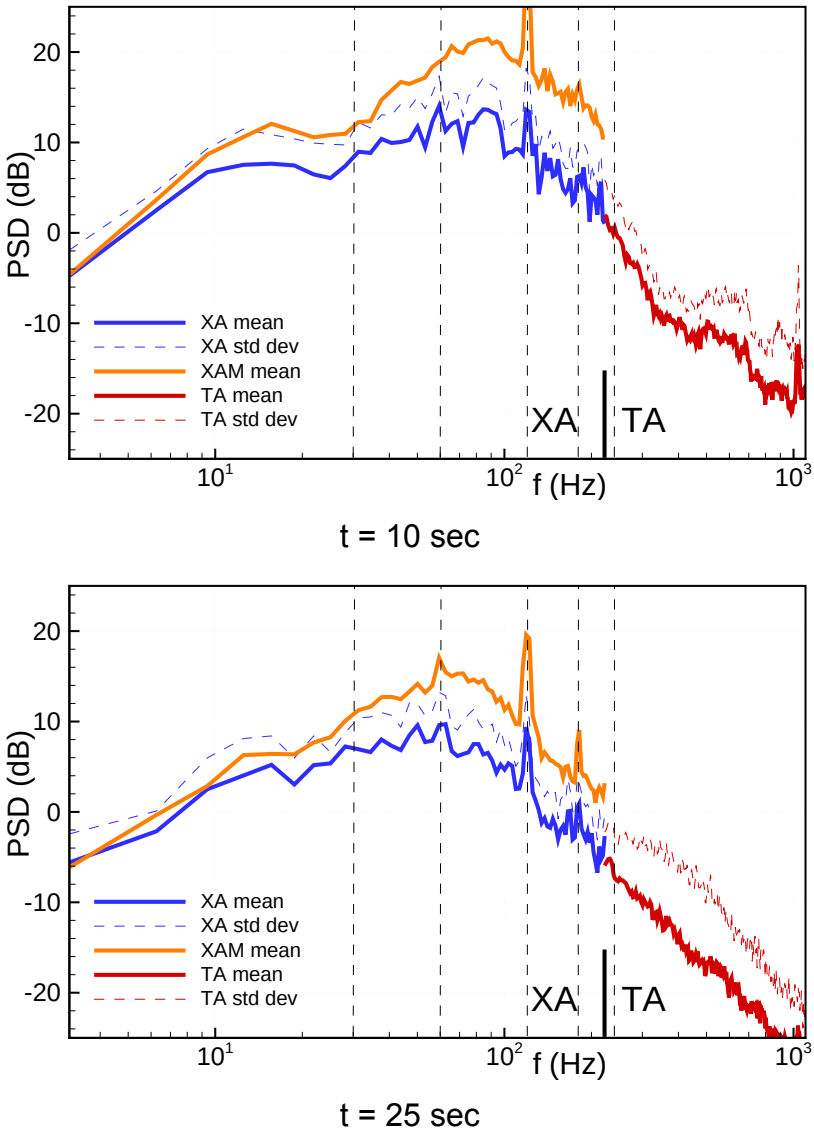

FIG 12: Average PSD of wake vortex noise of 13 flyovers of aircraft type B733 at 10 sec and 25 sec after flyover. The vertical, dashed lines indicate harmonics and sub-harmonics of the electric power supply frequency causing the narrow peaks.

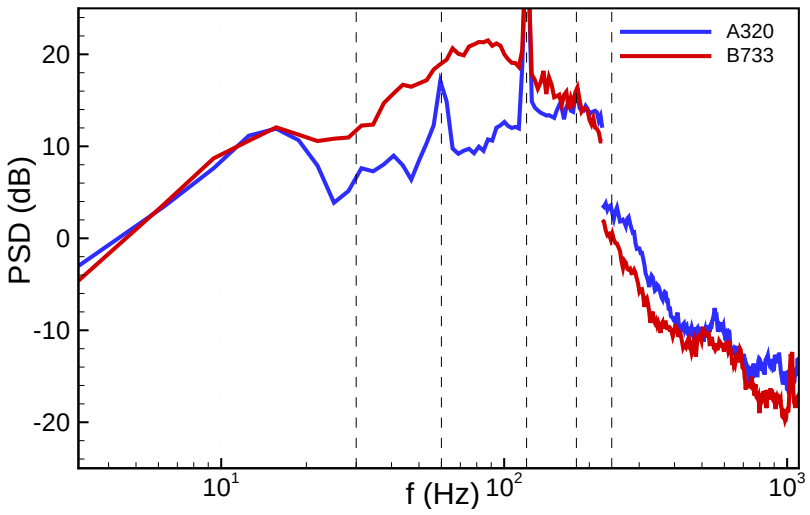

t = 10 sec

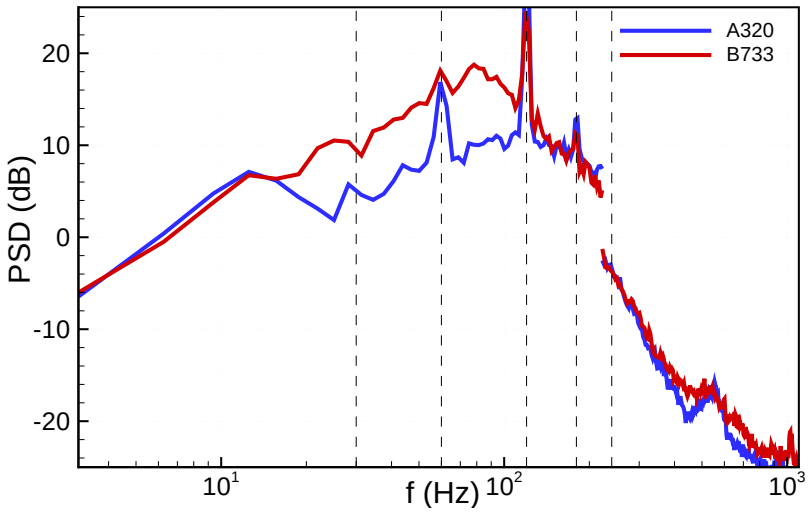

t = 20 sec

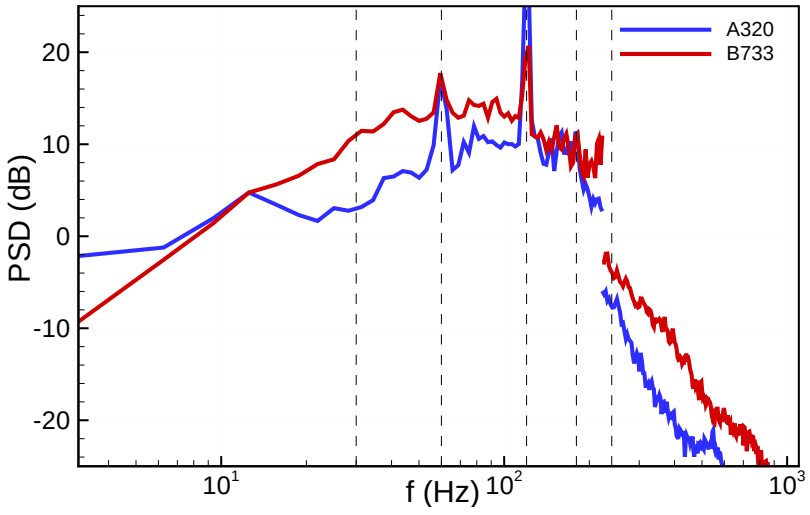

t = 30 sec

FIG 13: Comparison of the averaged wake vortex noise PSD_p behind the aircraft types A320 and B733 at different time after fly-over

FIG 13 shows the PSD_p -spectra for both of the types A320 and B733 at t = 10, 20, and 30 sec after flyover. The spectra were obtained by averaging the focused spectra of 12 A320 and 13 B733 flyovers. The frequency range f < 220 Hz is covered by the XA and f > 220 Hz by the TA. The spectra have similar levels below f < 12 Hz and above f > 220 Hz. The levels in the frequency range between differ significantly. The wake vortices of the B733 aircrafts are up to 10dB louder than the wakes of the A320 which is in agreement with the personal impression made in field test.

By comparing the averaged PSD_p of all aircraft types it was found the wake vortex noise spectra are either similar to the spectra of the A320 or to the B733. Two groups of aircraft with similar spectral vortex noise characteristics have been defined. The first class includes the types A319, A320, BA46, and CRJ200 and the second B733, B734, B735, B738, B752, and MD80. This surprising result needs to be confirmed by future measurements. The average wake vortex noise PSD_p at t = 20 sec of all aircraft types belonging to group 1 and 2 are plotted in **FIG 14** and **FIG 15** respectively.

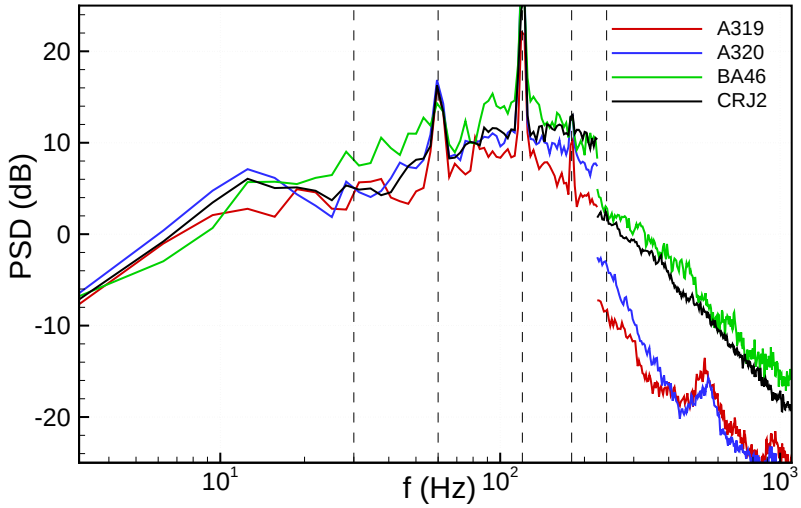

FIG 14: Averaged wake vortex noise PSD_p at t = 20 sec after flyover of group 1 aircraft types

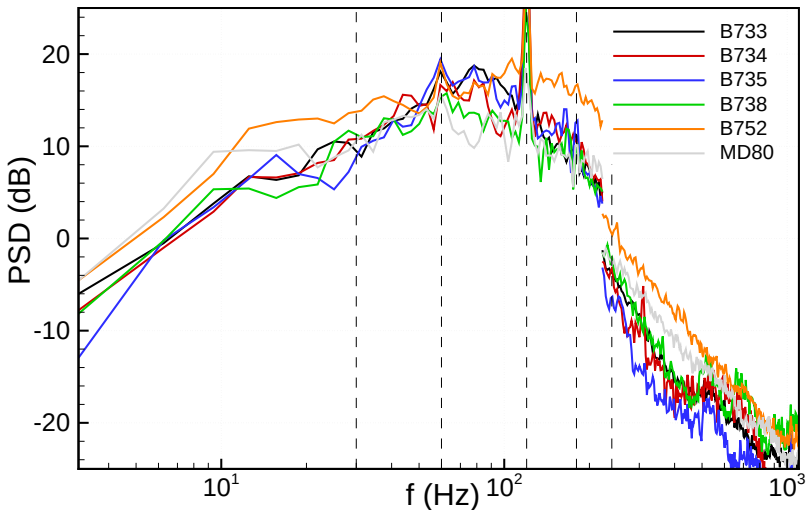

FIG 15: Averaged wake vortex noise PSD_p at t = 20 sec after flyover of group 2 aircraft types

The numerical study of the wake vortex noise suggested the relation $f_a \approx f_r = \Gamma / (2\pi r_c)^2$ between the vortex core rotation frequency f_r and the frequency of the peak level f_a in the noise spectra. According to this relation the rotation frequency is very sensitive to the estimated core radius.

TAB 1 summarizes the aircraft parameters and lists the resulting rotation frequencies of the core depending on its radius r_c = 0.06 B or r_c = 0.01 B which were reported in numerical and experimental wake vortex studies [16]. The range of the resulting frequencies estimated in **TAB 1** makes clear that both of the maxima found in the noise spectra can be related to the core rotation frequency by adjusting the core radius. The existing data base does not give sufficient evidence to draw a final conclusion about the components of the wake vortex noise spectra.

TAB 1: Aircraft and wake vortex parameters

a/c type	Wing span B m	Landing mass x10³ kg	Γ m²/s	f_r 6%B Hz	f_r 1%B Hz
A319	34.1	54.0	240.1	1.5	52.3
A320	34.1	57.4	255.2	1.6	55.6
B733	28.9	47.2	247.9	2.1	75.3
B734	28.9	50.6	265.6	2.2	80.7
B735	28.9	44.1	231.7	2.0	70.4
B738	34.3	59.3	262.1	1.6	56.4
B752	38.1	77.7	309.5	1.5	54.1
B763	47.6	110.7	352.6	1.1	39.5
B772	60.9	173.4	431.3	0.8	29.4
BA46	26.3	32.4	186.6	1.9	68.3
CRJ2	21.2	19.1	136.6	2.1	76.9
MD80	32.9	54.2	250.1	1.6	58.6

The core rotation frequency is expected to decrease as wake vortex ages. This is due to the decaying circulation and the increasing core size caused by diffusion. If the frequency at the peak level in the wake vortex noise spectra is a function of the core rotation frequency as found in the numerical study, the peak level should move towards lower frequencies as the wake vortex ages. Assuming the core growth is negligible, the frequency shift becomes only a function of time weighted by the circulation decay as stated in equation (6). The average circulation decay was derived from LIDAR results for each aircraft type.

$$f = (\Gamma_0 + \dot{\Gamma} t) / (2\pi r_c)^2 \qquad (6)$$

FIG 16 compares the expected frequency shift f_2 of the second peak level according to equation (6) (solid lines) with the shift observed in the averaged wake vortex noise PSD_p (dashed lines) behind the aircraft types A320, B733, B752 and CRJ2. The shifts measured for the aircraft types B733 and B752 match the model predictions but show an unexpected behaviour for the aircraft types A320 and CRJ2. The mismatch for the latter types might be caused by a wrong determination of the initial frequencies at t = 5 sec which seem to be too high for the types A320 and CRJ2.

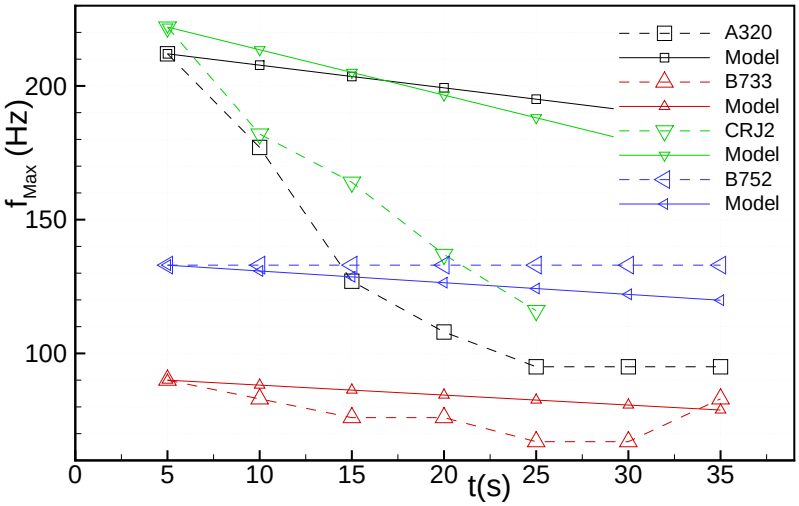

FIG 16: Predicted and measured frequency shift of the second maximum in wake vortex noise spectra for the aircraft types A320, CRJ200, B733 and B752

5.6. Single microphone data

During the field measurements sequences of audible sharp whipping noise events were regularly observed between t = 10 to 40 sec after the flyover. These acoustic events which were associated with bursting or linking of the vortices are also detectable in the recorded sound pressure time signals of single microphones. In **FIG 17** the time history of 1/3-octave band filtered sound pressure levels are plotted. In the frequency bands f = 250 Hz to f = 400 Hz a sudden level increase at about t = 20 sec happens which is followed by a fast level decrease. This event was clearly correlated with a whipping noise event by replaying the source track via loudspeakers.

Although these noise events are associated with vortex busting or linking they definitely do not provide a reliable indication of a final wake vortex break up. Moreover, a correlation between the sound pressure time histories and the sound source distributions revealed that the typical vortex noise signature in the localisation map disappeared after the noise event but reappeared only a few second later. This observation was confirmed by LIDAR data.

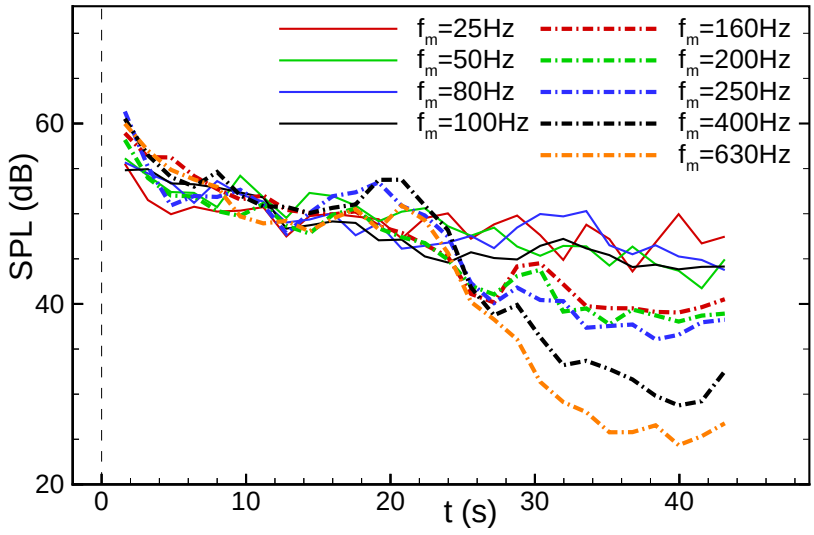

FIG 17: Time history of 1/3-octave filtered sound pressure signal of a single microphone after the flyover of a CRJ2 aircraft

6. CONCLUSIONS

The noise emission of aircraft wake vortices has been studied experimentally in several measurement campaigns at airports and investigated numerically using LES and an acoustic analogy method.

The numerical study of wake vortex noise suggests that:

1) The strongest sound sources are located close to vortex cores.
2) The frequency of peak level in noise spectra is related to the rotation frequency of vortex cores, $f_a \approx f_r = \Gamma / (2\pi r_c)^2$.

The experimental results showed that:

1) The sound sources of aircraft wake vortices are located close to or at the vortex cores.
2) The two vortices can be detected and tracked separately in the sound source localisation maps.
3) The source strength varies along vortex axes and is highly unsteady.
4) The focused wake vortex noise has probably two maxima: The origin of the first maximum at $f_1 \approx 10$ Hz has not been identified. The origin of second maximum at $f_2 \approx 100$ Hz are wake vortices.
5) The wake vortex noise spectra depend on the wake generating aircraft type: The aircraft could be categorized into two classes depending on the noise spectrum of the generated wake vortex.
6) A sudden noise event observed in the field tests is probably related to vortex bursting or linking but does not reliably indicate a final vortex break up.

Although, the wake vortex detection capability of LIDAR is superior, technologies based on the vortex noise emission remain interesting as they are complimentary and have the potential for further performance improvements.

Acknowledgments. Parts of the wake vortex simulation data used in this work have been obtained within the European research project AWIATOR (Contract G4RD-CT2002-00836).

REFERENCES

[1] International Civil Aviation Organisation: *Air Traffic Service Planning Manual II-5-3-2*, 1992.

[2] Gerz T., Holzäpfel F., Bryant W., Köpp F., Frech M., Tafferner A. and Winckelmans G.: Research towards a wake-vortex advisory system for optimal aircraft spacing, *Comptes Rendus Physique*, Académie des Sciences, Paris, **6**, No. 4-5, 501-523, 2005.

[3] Michel, U.; Böhning, P.: *Investigation of Aircraft Wake Vortices with Phased Microphone Arrays*, 8th AIAA/ CEAS Aeroacoustics Conf., AIAA 2002-2501, 2002.

[4] Böhning, P.; Michel U.: *Detektion von Wirbelschleppen mittels Mikrofon-Arrays*; DGLR 2004-015, 2004.

[5] Dougherty, R.; Wang, F.; Booth, E.; Watt M.; Fenichel, N.; D'Errico, R.: *Aircraft Wake Vortex Measurements at Denver International Airport*, 10th AIAA/CEAS Aeroacoustics Conf., AIAA 2004-2880, 2004.

[6] Booth, E.; Humphreys, W.: *Tracking and Characterization of Aircraft Wakes using Acoustic and Lidar Measurements*, 11th AIAA/CEAS Aeroacoustics Conf., AIAA Paper 2005-2964, 2005.

[7] Wang, F.; Wassaf, H.; Gulsrud, A.: *Acoustic Imaging of Aircraft Wake Vortex Dynamics*, 23th AIAA/CEAS Applied Aerodynamics Conf., AIAA 2005-4849, 2005.

[8] Fine, N., Kring, D.: *Opto-Acoustic Tracking of Aircraft Wake Vortices*, 11th AIAA/CEAS Aeroacoustics Conf., AIAA 2005-2965, 2005.
[9] Holzäpfel, F.: *Probabilistic Two-Phase Wake Vortex Decay and Transport Model*, J. Aircraft, **40** (2), 2003.
[10] Zheng, Z.; Wenhua L.; Wang F.; Wassaf H.: *Influence of Vortex Core on Wake Vortex Sound Emission*, 12th AIAA/CEAS Aeroacoustics Conf., AIAA 2006-2538, 2006.
[11] Holzäpfel, F.; Hofbauer; T.; Darracq; D., Moet; M.; Garnier, F.; Gago, C.: *Analysis of wake vortex decay mechanisms in atmosphere*, Aerospace Science and Technology, Vol. **7**, 2003.
[12] Rossow, V.: *Lift-generated vortex wakes of subsonic transport aircraft*, Progress in Aerospace Science **35**, 507-660, 1999.
[13] Donaldson, C., Bilanin, A.: *Vortex wakes of conventional aircraft*, AGARDograph 204, 1975.
[14] Holzäpfel F., Gerz T., Baumann R.: *The turbulent decay of trailing vortex pairs in stably stratified environments*, Aerospace Science Technology, vol. **5**, 95-108, 2001.
[15] Jeong, J., Hussain, F.: *On the identification of a vortex*, J. Fluid Mech., **285**, 69-94, 1995.
[16] Delisi, D.; Greene G.; Robins, R.; Vicroy, D.; Wang, F: *Aircraft Wake Vortex Core Size Measurements*, 21th AIAA/CEAS Applied Aerodynamics Conf., AIAA 2003-3811, 2003.
[17] Powell, A., *Theory of vortex sound*, Journal of the Acoustical Society of America, vol. **36**, 177-195, 1964.
[18] Howe M. S., *Theory of Vortex Sound*, Cambridge University Press, 2003.
[19] Möhring, W.: *On vortex sound at low Mach number*, J. Fluid Mech. **85**(4), 685-691, 1978.
[20] Elias, G.: *Source Localisation with a Two-Dimensional Focused Array: Optimal Signal Proces-sing for a Cross-Shaped Array*; Inter-Noise 95, 1995.
[21] Dougherty, R.: *Advanced Time-domain Beamforming Techniques*; 10th AIAA/CEAS Aeroacoustics Conf., AIAA- 2004-2955, 2004.
[22] The Airline Codes Web Site: *IATA Aircraft Type Codes*; http://www.airlinecodes.co.uk/acrtypes.htm

APPENDIX A

The ICAO aircraft type codes [22] are explained in TAB 2

TAB 2: IATA aircraft type codes

ICAO Code	Aircraft manufacture and type
A319	Airbus A319
A320	Airbus A320
B733	Boeing 737-300
B734	Boeing 737-400
B735	Boeing 737-500
B738	Boeing 737-800
B752	Boeing 757-200
B763	Boeing 767-300
B772	Boeing 777-200
BA46	British Aerospace BAe 146
CRJ2	Canadair Regional Jet 200
MD80	McDonnell Douglas MD80